Anion adsorption, $Ti_3C_2T_z$ MXene multilayers and clay-like swelling

Cooper A. Voigt[†], Michael Ghidiu[†], Varun Natu[†], Sankalp Kota[†] and Michel W. Barsoum[† *].

† Department of Materials Science and Engineering, Drexel University, Philadelphia, Pennsylvania 19104, United States

Supporting Information Placeholder

ABSTRACT: MXenes are a relatively new and large family of two-dimensional (2D) early transition metal carbides derived typically by etching the MAX phases in fluoride containing solutions. While numerous studies have investigated the role of cations on the interlayer distance, d_{0002}, between MXene multilayers (MLs) very little is known about the role of anions. Herein, using mainly X-ray diffraction (XRD), the effect of anions on d_{0002}, of $Ti_3C_2T_z$ MLs, where T represents various terminations, was systematically studied. The MLs were produced by etching Ti_3AlC_2 powders in hydrofluoric (HF) acid alone or in mixtures of HF and mineral acids with anions larger than F, viz. hydrochloric, hydrobromic, hydroiodic, sulfuric or phosphoric acids. The nature of the cations present in the post-etching washing solutions were also varied. The results show that the presence of the larger anions demonstrably facilitates water intercalation and de-intercalation. The fact that, for the most part, d_{0002} in fully dried MLs are not a function of mineral acid, together with post-etching chemical analysis with energy dispersive spectroscopy and X-ray photoelectron spectroscopy (XPS) showing that the amount of residual anions after etching was quite small – in some cases vanishingly so – leads to the conclusion that the larger anions do not enter the interlayer space, but most probably preferentially adsorb onto the positively charged ML edges, keeping the interlayer space open which, in turn, eases water intercalation and de-intercalation.

Introduction

MXenes are a relatively new family of two-dimensional (2D), materials synthesized from the MAX phases typically *via* etching in fluorine-containing solutions such as hydrofluoric acid, HF,[1,2] hydrochloric acid, HCl and lithium fluoride, LiF,[3] and others.[4,5] The MAX phases, in turn, are atomically layered, ternary carbides and nitrides that have a general formula $M_{n+1}AX_n$, where M is an early transition metal (Ti, V, Mo, Nb, Cr etc.), A is a select element from groups 13-16, X is carbon and/or nitrogen, and $n = 1, 2$ or 3.[6] Upon etching, the A layers – most often Al – are replaced by surface terminations, such as –OH, –F and –O, to create a multi-layered (ML) MXene with a formula, $M_{n+1}X_nT_z$, where T_z represents the surface terminations. HF-etched MLs are composed of stacks of $M_{n+1}X_nT_z$ sheets held together by hydrogen bonding and Van der Waals forces.[7] Since their discovery in 2011 [1], MXenes have shown great promise in applications such as energy storage [3,8–16], water purification[17–19], transparent conductive electrodes[5,20–23], polymer nanocomposites [24], electromagnetic shielding [25,26], piezoresistive sensors [27] and more[16].

In many MXene applications, understanding the nature of the cation/water/interlayer space interactions is important. Cation intercalation has attracted much attention since spontaneous intercalation along with impressive electrochemical performance[3,11] and basal swelling was demonstrated[11]. Furthermore, cation intercalation is a prerequisite for many delamination techniques needed to achieve aqueous, colloidal suspensions that are then used to fabricate filtered or other films[17,28].

Spontaneous intercalation of cations and basal swelling in MXenes prompted their comparison to silicate clays and some transition metal dichalcogenides [3,29], where hydration of the metal cations in the interlayer space causes expansion of the basal spacing as evidenced by a shift to lower angle 2θ of the (00l) peaks in X-ray diffraction (XRD) patterns. For the most part, basal swelling in cation-intercalated clays and MXenes follows a discrete pattern during hydration that is roughly attributed to 0, 1, or 2 water layers (WLs) with interlayer distances of ~10 Å, ~12.5 Å, 15-16 Å in $Ti_3C_2T_z$, respectively, between the 2D sheets, depending on the cationic hydration enthalpy and humidity of the environment [29–33].

The bulk of this work in based on the position of the (0002) MXene peak in XRD patterns. Since the spacing associated with this peak is half the c-lattice parameter, it will henceforth be referred to as d_{0002}.

One of the defining features of Li^+-intercalated, clay-like $Ti_3C_2T_z$ is that it shows a 2 WL (≈ 16 Å) basal spacing when fully hydrated. However, there is a wide range of humidity over which the 1 WL basal spacing is more stable, and there are reports of Li-intercalated MXene in aqueous solutions that do not show full swelling to 16 Å, but stop at 12.5 Å [11,34,35]. Furthermore, electrochemically intercalating HF-etched $Ti_3C_2T_z$ electrodes with Li^+ resulted in a reduction in electrode thickness [35]. Therefore, a balance must exist between the, i) electrostatic attraction of the negatively charged $Ti_3C_2T_z$ sheets and the intercalated cations that causes contraction and, ii) cationic hydration shells that cause clay-like swelling. Access to $Ti_3C_2T_z$ interlayer must also be kept open by intercalated water or cations to allow further intercalation or cation exchange[29]. The factors affecting whether Li^+-intercalation causes swelling or contraction are not well understood.

Critically, reports of clay-like swelling were of $Ti_3C_2T_z$ etched in either HCl and LiF, or HF and LiCl solutions. Reports of basal contraction upon electrochemical Li^+ intercalation were of $Ti_3C_2T_z$ etched in HF alone. Kajiyama et. al.[36] showed improved electrochemical performance in Ti_2CT_z and $Ti_3C_2T_z$ etched with HCl-LiF[3], compared to etching in HF alone and attributed this improved performance to increased Li^+ access to the interlayer by steric chloride terminations propping open the MXene layers.

In short, the vast majority of work on $Ti_3C_2T_z$ MLs explored how cations affect the interlayer spacing. As far as we are aware, and

with the exception of Kajiyama et al.'s paper[36], there have been no studies on the effect of anions in the etching process. The purpose of this study is to determine whether anions play a role during etching of Ti_3AlC_2 and, if so, what their role is. Herein we describe the first systematic study of how large anions, *viz*. chlorine, Cl^-, bromine, Br^-, iodine, I^-, phosphate, $(PO_4)^{-3}$ and sulfate, $(SO_4)^{2-}$ affect d_{0002} of ML $Ti_3C_2T_z$. The latter were introduced by mixing HF with HCl, hydrobromic, HBr, hydroiodic, HI, sulfuric, H_2SO_4, or phosphoric, H_3PO_4, acids.

Experimental Details

Previously, MXenes etched in the presence of Cl^- were simultaneously intercalated with Li^+ via the HCl-LiF method[3] or the HF-LiCl method[29]. Herein, the experiments were designed in such a way as to decouple the effects of Li^+ intercalation from the effects of anion adsorption. Figure 1 is a schematic illustrating how that was accomplished. Powders of Ti_3AlC_2 were etched with HF alone, or with mineral acid (MA) mixtures of HF+HCl, HF+HBr, HF+HI, HF+H_3PO_4, or HF+H_2SO_4 and then washed in either deionized, nominally 18 MΩ water or in aqueous Li-salt solutions. By separately varying the etching and washing solutions, the effects of different anions on d_{0002} were separated from Li^+ intercalation. The resulting MLs were then characterized under various hydration/drying conditions *via* XRD and energy dispersive spectroscopy (EDS) in a scanning electron microscope.

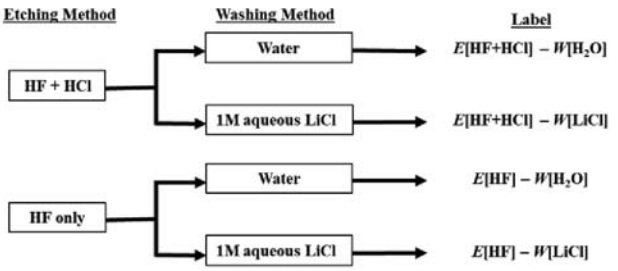

Figure 1. Schematic of etching and washing methods to separate the effects of anions and cations. Other anions can be substituted wherever Cl appears for MLs processed with those anions.

Synthesis of Ti_3AlC_2: Ti_3AlC_2 powder was synthesized by heating a ball-milled mixture of TiC, Al, and Ti (All from Alfa Aesar, Ward Hill, MA) in 2TiC:1.05Al:1Ti stoichiometry in an alumina, Al_2O_3, tube furnace under flowing, ultra-high purity argon, Ar, (AirGas, Cherry Hill, NJ, USA), at a rate of 5 °C/min to 1350 °C and holding for 2 h. The lightly sintered, porous Ti_3AlC_2 compact was then milled into a powder using a TiN-coated end mill on a drill press and then sieved to obtain a powder of particle size < 38 µm. The powder of particle size > 38 µm was ball milled for 24 h and re-sieved through 38 µm sieve to obtain more fine-grained powder that was then added to the original batch.

Low anion concentration $Ti_3C_2T_z$ synthesis: 4 g of Ti_3AlC_2 powders were added to 40 ml of 10 wt.% HF ("HF-"). For Cl, Br and I-etched $Ti_3C_2T_x$, the etchant was mixed nominally as a 10 wt.% HF concentration solution with a 5:1 MA:Al molar ratio (Table S1). The acid etchant mixture and Ti_3AlC_2 powder were stirred at room temperature (~25 °C) for 24 h.

After etching, distilled, nominally 18 MΩ H_2O was added to all samples until their volume was 90 ml, centrifuged for 2 min. at 3500 rpm and then decanted. Each sample was then split into two: One batch was washed in water *alone*, the other washed with an aqueous Li-salt solution. For washes 2 through 4, the Li-salt washed samples were washed with 1 M solutions of their respective Li-salt, viz. LiCl, LiBr or LiI. For washes 5, 6, and 7, all samples were washed with water alone. All samples were agitated by a vortex agitator to disperse the sediment before centrifuging.

High anion concentration $Ti_3C_2T_z$ synthesis: Half a gram of Ti_3AlC_2 powders were added to a mixture of 4.6 mL 48 wt.% HF and 17.9 mL distilled H_2O for a nominal 50:1 HF:Al ratio as a control. For the HCl, HBr, HI, H_3PO_4, or H_2SO_4 containing etchants, a mixture of HF + the corresponding mineral acid was mixed in a ratio of 50:1 HF:Al and 50:1 MA:Al and the remaining volume was topped with distilled H_2O up to 22.5 mL (Table S6). The concentration of MA in solution is nominally 5.7 M.

After etching, distilled, nominally 18 MΩ H_2O was added to all samples until their volume was 45 ml. All samples were then washed 5 times with water only. All samples were agitated by a vortex agitator to disperse the sediment before centrifuging.

Drying Protocols: To shed more light on the effect of anions on d_{0002}, the MLs produced herein were subjected to varying drying protocols. One set of samples was heated in a vacuum oven to 60 °C for 48 h, followed by a 100 °C for 30 h and lastly at 150 °C for 14 h. Another set of samples was placed in a desiccator containing P_2O_5 and $CaSO_4$ under vacuum at room temperature for 48 h followed by heating to 150 °C for 12 h also under vacuum. In all cases the vacuum level was ≈ 0.2 atm.

X-Ray Diffraction (XRD): A Cu K_α radiation source diffractometer (λ = 1.54 Å) (Rigaku SmartLab, Rigaku, Tokyo, Japan) was used to obtain all XRD patterns with a step size of 0.02° and a dwell time of 2 s per step.

Maintaining full hydration of the "fresh" $Ti_3C_2T_z$ powders, while performing XRD required the following procedure: The wet $Ti_3C_2T_z$ sediment from the bottom of the centrifuge tube, covered in ~10 mL distilled H_2O, was scooped out and made flush with the powder sample holder of the XRD. A few milliliters of distilled H_2O were then gently dropped onto the wet powder until a visible meniscus formed. Excess distilled H_2O was then scraped off with a spatula so that the sample was again flush with the sample holder but maintained a visible water layer. The sample was then placed into the diffractometer for measurement. After measurement, the sample was visually inspected to confirm that a layer of water was still present, ensuring the sample had not dried out. See figure S7 for pictures of XRD sample preparation.

SEM and EDS: Dried MLs were pressed at a load corresponding to a stress of ~100 MPa to form free standing ≈ 1 mm thick discs which were then mounted on aluminum SEM stubs with double-sided carbon tape. SEM and EDS were performed on a Zeiss Supra 50VP (Carl Zeiss AG, Germany). Electron beam accelerating voltage of 20 kV was chosen to detect Br K_α emission lines due to the overlap of the Br L_α and Al K_α energies[37].

X-Ray Photoelectron Spectroscopy(XPS): XPS was performed using VersaProbe 5000 instrument (Physical Electronics, Chanhassen, Minnesota, USA). All the samples were sputtered using Ar-ion gun(1kV) for 2 mins. Pass energy of 23.5eV was used for all scans, with energy step of 0.025eV and step time of 500ms. The number of repeats per scan was set to 25.

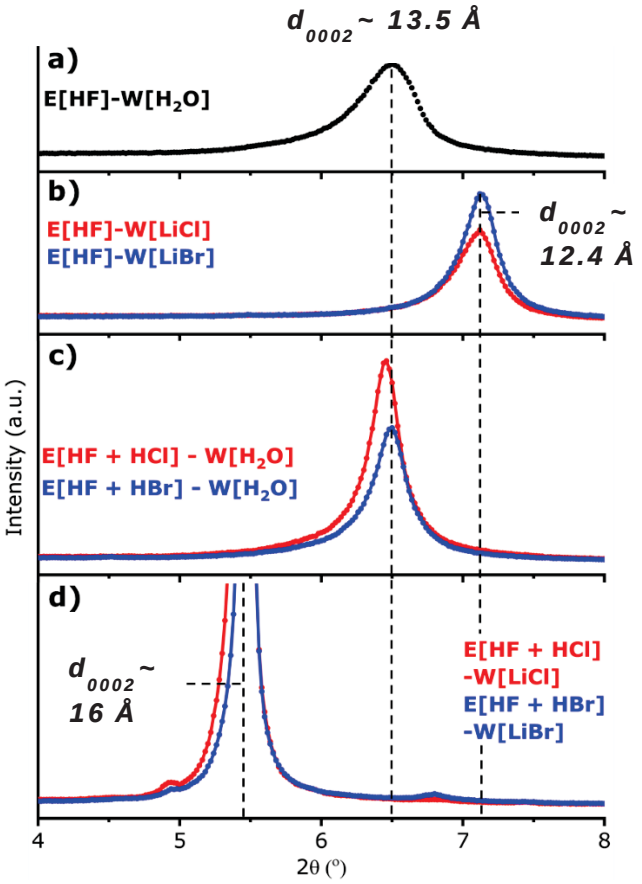

Figure 2. Low angle XRD patterns of fresh, never dried, $Ti_3C_2T_z$ MLs, a) HF-etched, water washed; b) same as a, but washed in LiCl (red) or LiBr (blue) solution after etching; c) HF+HCl (red) and HF+HBr (blue) etched and water washed; d) same as c) but washed in LiCl (red) or LiBr (blue) solution after etching.

Results

When Ti_3AlC_2 powders are etched in a 10 wt. % HF solution and then washed with water, the (0002) peak shifts from a corresponding *d*-spacing of 9.3 Å to 13.6 Å and broadens (Fig. 2a). When, instead of washing in water, the HF-only etched MLs are washed in 1 M LiCl three times, the d-spacing *decreases* from 13.6 Å to 12.4 Å, and the full width at half maximum, FWHM, decreases from 0.493° 2θ to 0.340° 2θ, indicating increased homogeneity along the *c*-axis (Fig. 2b). If instead of etching in HF alone, the Ti_3AlC_2 powders are etched in a 10 wt.% HF solution in the presence of HCl – added in a 5:1 HCl:Al ratio – and then washed in water alone, d_{0002} of the fresh, wet powder is the same as the HF-only etched viz. ≈ 13.6 Å (Fig. 2c). However, a notable decrease, from 0.493 to 0.206(4)° 2*θ*, in the FWHM of the (0002) peak is observed. If the HF + HCl etched MLs are instead washed in a 1M LiCl solution, d_{0002} expands to 16 Å (Fig. 2d) and spontaneous delamination of the material initiates. To test whether the swelling

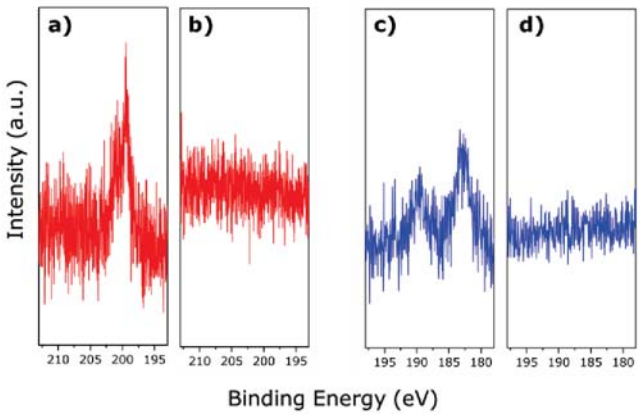

Figure 3. XPS of a) 5:1 Cl:Al ratio, E[HF +HCl] – W[H_2O] , b) E[HF] – W[LiCl], c) 5:1 Br:Al ratio, E[HF +HBr] – W[H_2O], d) E[HF] – W[LiBr].

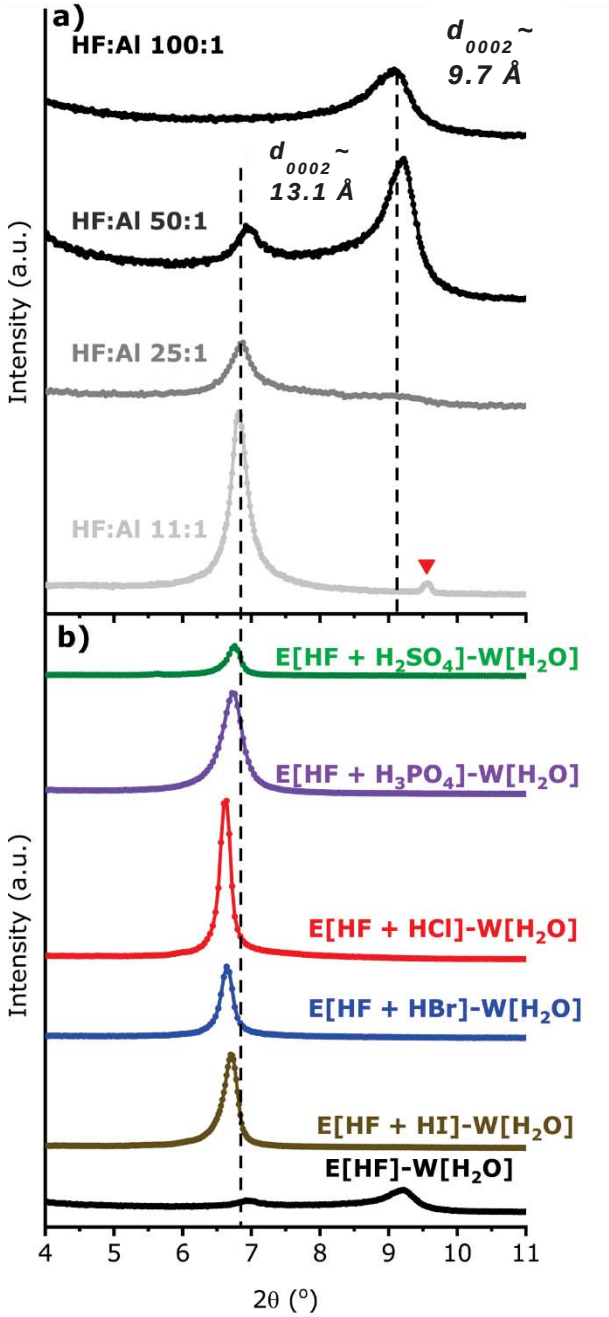

Figure 4. Low angle XRD patterns of MLs etched with, a) varying HF:Al ratios. Red triangle denotes Ti_3AlC_2 impurity (0002) peak. b) Swelling behavior of MLs etched in various mineral acids, MAs, in a 50:1 molar ratio of MA:Al and a 50:1 ratio of HF:Al.

effect is specific to Cl or could be achieved with other large anions, the same experiment was repeated with HBr and LiBr yielding similar results (Fig. 2, blue traces).

A Cl or Br signal is detected in XPS spectra of samples that were etched in the presence of Cl or Br, respectively (Figs. 3a, c). In contrast, this signal is absent when HF-only etched samples were washed in LiCl or LiBr, respectively (Figs. 3b & 3d). Trace amounts of Cl are also detected by SEM-EDS ($0.02_{\pm 1}$ per Ti_3C_2) in the MLs etched in the presence of Cl. The Br signal is too low to be reliably detected by EDS in MLs etched in 5:1 Br:Al (Table S2). XPS if the Br 3d and Cl 3d at high and low concentrations can be found in figure S8.

The effect of the HF:Al etchant ratio on swelling was studied by etching Ti_3AlC_2 powders in varying concentrations of HF-only from 100:1 to 11:1. XRD patterns on fresh wet, never dried MLs (Fig. 4a) show that d_{0002} for the 100:1 HF:Al ratio mixture (Fig. 4a, top curve) is ~ 9.7 Å. Reducing the HF:Al ratio by half to 50:1 HF:Al still results in the major (0002) peak centered at d_{0002} ~ 9.7 Å (Fig. 4a, second from top). However, in this case a minor peak appears at a 2θ corresponding to d_{0002} ~ 13 Å. When the ratio is further reduced to 25:1, the major (0002) peak is now centered at a 2θ angle corresponding to d_{0002} ~ 13 Å, with a broad hump extending to d_{0002} ~ 9.7 Å (Fig. 4a, third from top). Lastly, reducing the HF:Al ratio again to 11:1 results in a sharp, single peak centered at a d-spacing of ~ 13 Å.

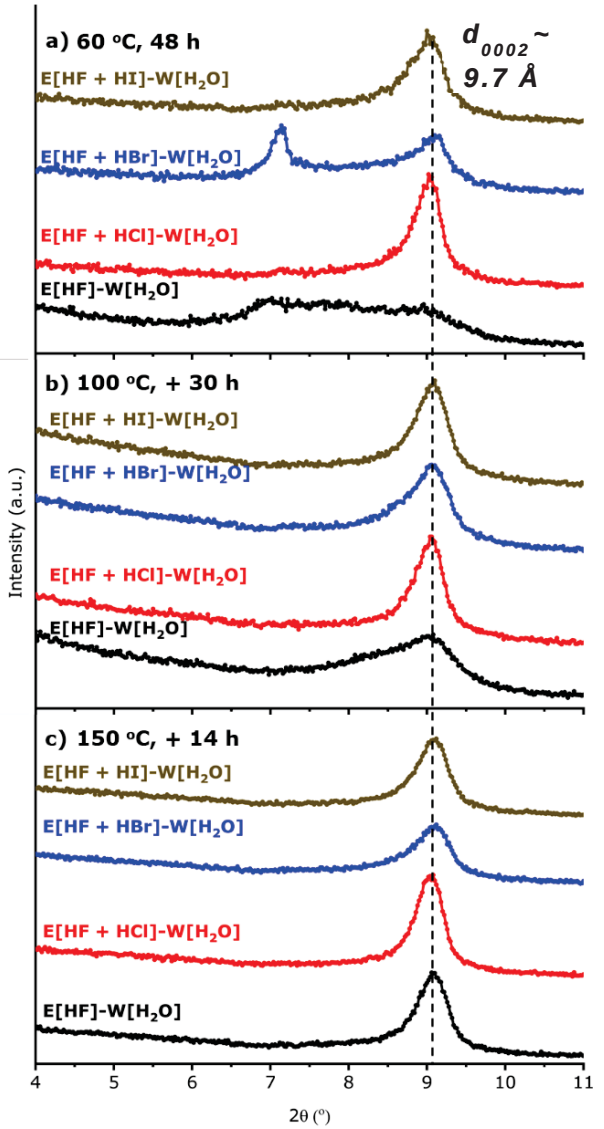

Figure 5. Low angle XRD patterns of MLs produced by etching in 5:1 MA:Al and 11:1 HF:Al solutions after drying, a) at 60 °C for 48 h followed by, b) 100 °C for 30 h followed by, c) 150 °C for 14 h. All drying was conducted under a ~ 0.2 atm mechanical vacuum.

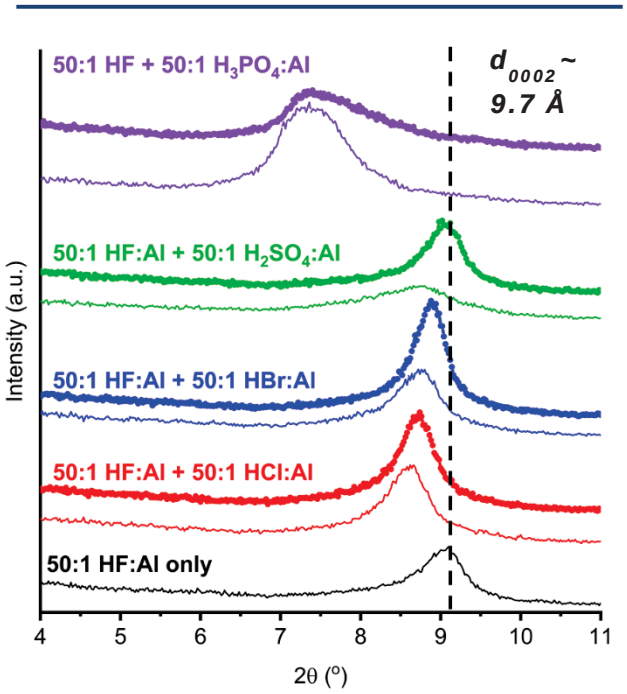

Figure 6. Low-angle XRD of 50:1 anion to Al concentration etched $Ti_3C_2T_z$ and dried at 25 °C in a desiccator under a ~0.2 atm mechanical vacuum. Thin lines are MLs dried under P_2O_5 and $CaSO_4$ at room temperature desiccant and a ~0.2 atm mechanical vacuum. Bold lines are MLs dried an additional 12 h at 150 °C under ~0.2 atm mechanical vacuum.

Figure 4b is a plot of the XRD patterns of fresh MLs produced by etching the MAX powders in a 50:1 ratio of HF:Al *and* MA:Al etchant, where MA is HCl, HBr, HI, HF, H_3PO_4, or H_2SO_4. In all cases, the MLs, swell readily to d_{0002} ~ 13 – 13.5 Å. Figure S6 shows that at high H_2SO_4:Al ratios, a peak corresponding to d_{0002} ~ 19 Å appears.

XRD patterns of the low MA concentration (5:1) samples was then taken after drying out in 3 steps at increasing temperatures (Fig. 5). Figure 5a shows the resulting XRD patterns after drying under the relatively mild conditions of 60 °C for 48 h in vacuum (≈ 0.2 atm) After this treatment, the HF-only etched MLs show a broad hump (Fig. 5a, black line) extending from 7° to 9° 2θ, or d_{0002} between ~ 12.5 Å and 9.7 Å. In sharp contrast, the d-spacing of the MLs etched in a HF+HCl or HF+HI mixture collapse to d_{0002} ~ 9.7 Å (Fig. 5a, red and brown lines). The sample etched in a HF+HBr mixture showed two peaks (Fig. 5a, blue line).

The same powders were then placed back in the vacuum oven at 100 °C for more 30 h. After this drying treatment, d_{0002} was ≈ 9.7 Å, for all HF + MA etched MLs (Fig. 5b). It was only by placing the same powders, one last time, into the vacuum oven, at 150 °C for 14 h that the (0002) peak of the HF-only etched MLs were finally centered at ~9° 2θ, or d_{0002} ~ 9.7 Å with a FWHM that was comparable to the others (Fig. 5c).

Table 1 – SEM/EDS of 50:1 MA: Al ratio MLs

Element	HF + HCl	HF + HBr	HF + HI	HF + H_3PO_4	HF + H_2SO_4
Ti	3	3	3	3	3
Al	0.025(9)	0.01(1)	0.053	0.020(4)	0.020(2)
C	2.17(7)	1.94(3)	2.37	1.95(2)	2.02(7)
O	1.10(9)	1.01(8)	0.892	2.00(7)	1.15(3)
F	1.59(6)	1.53(2)	2.23	1.19(4)	1.56(3)
Cl	0.124(4)	0	0	0	0
Br	0	0.044(7)	0	0	0
I	0	0	0.021	0	0
P	0	0	0	0.041(1)	0
S	0	0	0	0	0.0104(5)

In another set of experiments, the MLs produced by etching in a 50:1 ratio of HF:Al *and* MA:Al etchant (Fig. 6) were dried in a desiccator filled with phosphorous pentoxide, P_2O_5 and calcium sulphate, $CaSO_4$, desiccants and a ~ 0.2 atm vacuum at room temperature for 48 h (Fig. 6, thin traces). The same samples were then further dried at 200 ºC under ~ 0.2 atm vacuum for 12 h (Fig. 6 bold trace). Drying of these MLs results in d_{0002} ~ 9.7–10.2 Å (Fig. 6, thin lines) for all MAs except phosphoric acid. Drying the same powders an additional 12 h at 200 ºC under < 0.2 atm mechanical vacuum only shifts the peaks to slightly lower d_{0002} values. It is worth noting here that with the exception of the MLs etched in the presence of H_2SO_4, all other (0002) peaks are downshifted relative to the fully dried HF only etched sample. Compare the thin vertical black lines that are guides to the eyes in Figs. 5 and 6.

At the higher MA concentration (50:1 MA:Al) all anions could be detected by EDS (Table 1).

Discussion

This work's most important finding is that anions – despite not intercalating into the interlayer space (see below) – still play an important role in facilitating the swelling and drying of $Ti_3C_2T_z$ MLs. A schematic of what is postulated to occur in shown in Fig. 7. In the remainder of this discussion we make our case.

Figure 2 demonstrates that in the absence of Li^+, d_{0002} ~ 13.6 Å (Fig. 2a and c). This state of spacing is henceforth taken as our reference state because there are no cations between the layers. When the HF-only etched MAX phase is washed with LiCl, d_{0002} shrinks to ≈ 12.4 Å (Fig. 2b). If the samples are etched in the presence of HCl or HBr, and then washed in a Li^+ containing solution, *viz*. LiCl, d_{0002} expands to ~ 16 Å (Fig. 2d). This is an important result because it clearly demonstrates that the presence of large anions *during* etching greatly influences d_{0002}. The contraction to 12.4 Å seemingly contradicts reports where the d-spacing of Li^+-intercalated $Ti_3C_2T_z$ etched in HCl-LiF or HF-LiCl solutions expand to d_{0002} ~ 16 Å when fully hydrated[3,29]. However, the shrinkage is consistent with reports where electrochemical Li^+-intercalation into HF-only etched $Ti_3C_2T_z$ caused a decrease of electrode thickness ascribed to the electrostatic attraction between the negatively-charged $Ti_3C_2T_z$ layers and the positively charged Li^+ cations[35]. It is thus reasonable to conclude that the presence of Cl^- - most probably adsorbed onto the edges (see below) - during etching is having a steric effect[36] that keeps the interlayer space propped open, facilitating not only Li^+ intercalation, but also its water of hydration causing expansion (Fig. 7, right panel).

The results displayed in Fig. 4a show that as the HF:Al ratio is decreased, d_{0002} of the fresh, wet powders increases from 9.7 Å to ~ 13.1. A few studies have compared $Ti_3C_2T_z$ etched at different HF concentrations and shown a d-spacing increase at lower HF concentrations and attributed this increase to intercalated water[7,38,39]. Decreasing the F:Al ratio in the etchant has been shown to increase the ratio of O:F terminations on $Ti_3C_2T_z$ MLs[40] and Wang et al. concluded that the interlayer hydrogen bonding in $Ti_3C_2T_z$ MLs was stronger when etched in 10 wt.% HF *vs.* 50 wt.% HF[7]. If the strength of interlayer hydrogen bonding increases with increasing O:F termination ratio, the hydrophilicity of the $Ti_3C_2T_z$ sheets concomitantly increases[2], likely providing a greater driving force for water intercalation. The fact that adding anions to the etchant (Fig. 4b) leads to increased water intercalation suggests that, although the driving force for intercalation is likely weaker than in the case of intercalated Li^+ (Figs. 2b & d), these anions similarly facilitate water intercalation.

If anions indeed facilitate water ingress between the MXene sheets, then they should also facilitate its egress. A perusal of the XRD patterns shown in Fig. 5 clearly demonstrates that the d_{0002} of ~ 9.7 Å, i.e. complete water de-intercalation, is reached first by the HF-HCl and HF-HI etched MLs, followed by the HF-HBr MLs. Crucially, it is only by annealing at 150 ºC for 14 h that the HF-only etched MLs (lowest trace in Fig. 5c) are finally as dry as the others.

The fact that the HF-only etched MLs required a significantly more intense drying protocol to fully de-intercalate water compared to the HF+ MA samples is fully consistent with the schematic shown in the right panel in Fig. 7. Anions adsorbed at the edges likely prop open the edges and allow water molecules easier access both into and out of the interlayer. The fact that the 2θ values of *all* the peaks after intense drying are identical (Fig. 5c) is noteworthy since it strongly suggests that the anions do not intercalate between the layers.

The next question is what happens upon drying when the MA:Al ratio during HF etching is 50:1. Figure 6 shows that all MLs, with the exception of those etched in the presence of H_3PO_4, return to d_{0002} ~ 9.7 Å after drying at 150 ºC for 14h in vacuum. The HF+H_3PO_4 etched ML (0002) peak remains broad and centered at d_{0002} ~ 12 Å.

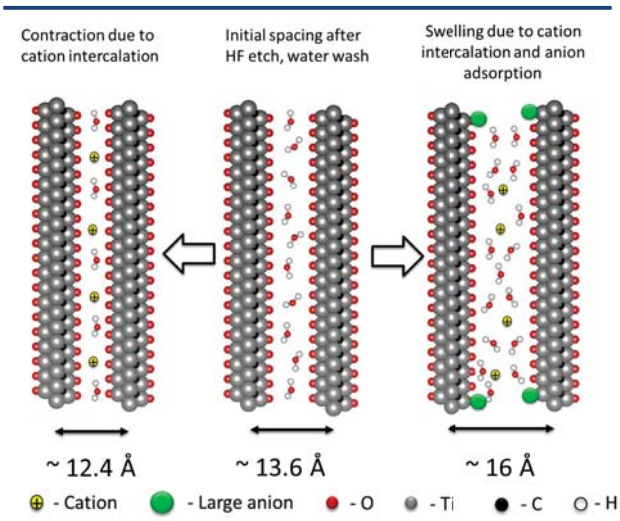

Figure 7: Schematic of the effect of anions on $d_{c/2}$. Central panel shows our ML reference state – with $d_{c/2}$ ~ 13.6 Å – obtained by HF-only etching. It is important to emphasize that these MLs were never dried. Left panel shows that if Li^+ is inserted into the reference state ***after*** etching, $d_{c/2}$ shrinks. If, however, the Li^+ is intercalated into $Ti_3C_2T_z$ etched in an HF + MA mixture, a $d_{c/2}$ of ≈ 16 Å is obtained.

Typically, when $Ti_3C_2T_x$ MLs are fully dried they cannot be re-hydrated or intercalated with cations.[29] However, when HF + H_3PO_4 etched MLs were immersed in water for 48 h after drying, a gradual increase in peak intensity corresponding to $d_{0002} \sim 12$ Å occurs, suggesting that water is re-intercalating the MLs (Fig. S1). This result suggests that some P-based species may have intercalated between the MLs. This leads to the last outstanding question in this work: Where are the anions located?

Based on the facts that for the MLs etched in low concentrations of MA, i) the d_{0002} values for the fully dried samples are identical to those etched in HF alone (Fig. 5c), ii) the anion concentrations measured in EDS were at most 0.02 per (Table S2) and the XPS signal for the anions was also quite weak, and iii) the swelling behavior observed in XRD (Fig. 2); it is reasonable to assume that the large anions are located at the ML edges. The MLs are shown schematically in the right panel of Fig. 7. When $Ti_3C_2T_z$ MLs are washed with Li^+ containing solutions, what occurs is quite telling. When the large anions are absent from the edges, the electrostatic attraction between the $Ti_3C_2T_z$ sheets themselves is probably too high for the Li^+ to enter the ML space with its full hydration shell (Fig. 2b). Any remaining Li^+ entering the interlayer space would then be unable to cause swelling to 2WL. The final spacing is thus closer to 1WL than 2WL. If large anions are adsorbed at the edges they might prevent the $Ti_3C_2T_z$ sheets from collapsing when Li^+ first enters the interlayer, allowing Li^+ to intercalate with its full hydration shell and cause basal swelling to 2WL. By adsorbing at the edges, the anions would have the greatest control over access to the interlayer at the relatively low concentrations we report in this work. Transmission electron microscopy (TEM) of single sheets to detect chemical inhomogeneity from the middle of the sheets to the edges is needed to verify this hypothesis.

In HF+HBr etched $Ti_3C_2T_z$ MLs, Br is difficult to detect at low concentration (5:1 MA:Al) in EDS due to overlap between the Al Kα and Br Lα X-ray emission energies (Table S2). However, XPS shows that the same trend for Cl holds for Br in that Br is detected in HF + HBr etched $Ti_3C_2T_z$, whereas no Br is detected in HF-only etched, LiBr washed $Ti_3C_2T_z$ (Fig. 2e & 2f).

The situation for the samples etched in a large excess of MA (50:1) is slightly more ambiguous. After full drying at 200 °C, all but the H_3PO_4 etched samples, the d-spacings are slightly higher than the reference state (Fig. 6). The origin of this difference is not known at this time. Table 1 shows that the highest anion signal was for the HF+HCl etched MLs, but even in this case, there are only ≈ 0.12 Cl atoms per Ti_3C_2 (Table 1). The values for all others are at least a factor of 3 lower. Said otherwise, if anions are present between the MLs, their concentration is quite low, even when the MA:Al ratio in the etching solution is 50:1.[29,41]

We note in passing that previous EDS work on HF+LiCl or HCl+LiF etched $Ti_3C_2T_z$ reported the presence of Cl[3,29]. In those cases, at least a fraction of the Cl signal was ascribed to salt impurities. In our HF+HCl etched, water washed $Ti_3C_2T_z$, *no* salt is added at any time during the synthesis, which is possibly why we detect a very small signal.

At high concentration (50:1), of all the halogens, F adsorbs most readily onto $Ti_3C_2T_z$, followed by Cl, then Br, then I, a trend correlating with the respective electronegativity of each halogen. Therefore, as has been seen in some clays[42], the anionic species compete for adsorption sites on $Ti_3C_2T_z$ based on their electronegativity. The case of the polyatomic anions (PO_4^{3-} and SO_4^{2-}) is more complex and cannot be directly compared to the halogens. In $Ti_3C_2T_z$ MLs, and distinct from anionic adsorption onto clay edges, the anion adsorption must occur *during etching* to have the steric effect discussed here (Fig. S2).

It should be noted that 50:1 etched MLs are quite sensitive to impurity cations in solution – mere washing in tap water caused swelling to $d_{0002} \sim 16$ Å compared to $d_{0002} \sim 13$ Å when no cations were present in the 18 MΩ distilled water used herein (Figure S5).

While the overall trend of anion-facilitated intercalation is consistent throughout repeat experiments, XRD of E[HF]–W[LiCl] MLs and E[HF+MA] –W[H_2O] MLs immersed in water sometimes show a signal with convoluted peaks corresponding to both 1WL and 2WL (Figs. S3 and S4). Further work is needed to determine the equilibrium d_{0002} of Li^+ intercalated MLs and what other variables besides anion adsorption might be important for determining equilibrium.

Conclusions

The impact of anions on the intercalation and deintercalation behavior of $Ti_3C_2T_z$ is demonstrated here for the first time. Etching Ti_3AlC_2 in a mixture of HF and another mineral acid with anions larger than –F or –O viz. HCl, HBr, HI, H_2SO_4 or H_3PO_4, facilitates the intercalation and deintercalation of water. The effect is only seen, however, when the larger anions are present during etching. Increased anion adsorption occurred when the concentration of respective mineral acid was increased in the etchant and the amount detected by EDS also correlated with electronegativity of the anion. We suggest that these larger anions preferentially adsorb onto edge site of MXene MLs because of the marked effect on hydration properties despite their low concentrations.

ASSOCIATED CONTENT

Supporting Information

AUTHOR INFORMATION

Corresponding Author

barsoumw@drexel.edu

Notes

The authors declare no competing financial interests.

ACKNOWLEDGMENT

This work was funded by the Swedish Research Council (Grant # 621-2014-4890). The authors thank Louisiane Verger for EDS of some samples and Patrick West for his advice on the water sources at Drexel University.

REFERENCES

(1) Naguib, M.; Kurtoglu, M.; Presser, V.; Lu, J.; Niu, J.; Heon, M.; Hultman, L.; Gogotsi, Y.; Barsoum, M. W. Two-dimensional Nanocrystals Produced by Exfoliation of Ti_3AlC_2. *Adv. Mater.* **2011**, *23* (37), 4248–4253.

(2) Naguib, M.; Mashtalir, O.; Carle, J.; Presser, V.; Lu, J.; Hultman, L.; Gogotsi, Y.; Barsoum, M. W. Two-Dimensional Transition Metal Carbides. *ACS Nano* **2012**, *6* (2), 1322–1331.

(3) Ghidiu, M.; Lukatskaya, M. R.; Zhao, M.-Q.; Gogotsi, Y.; Barsoum, M. W. Conductive Two-Dimensional Titanium Carbide "Clay" with High Volumetric Capacitance. *Nature* **2014**, *516* (7529), 78–81.

(4) Alhabeb, M.; Maleski, K.; Anasori, B.; Lelyukh, P.; Clark, L.; Sin, S.; Gogotsi, Y. Guidelines for Synthesis and Processing of 2D Titanium Carbide ($Ti_3C_2T_x$ MXene). **2017**.

(5) Halim, J.; Lukatskaya, M. R.; Cook, K. M.; Lu, J.; Smith, C. R.; Näslund, L.-Å.; May, S. J.; Hultman, L.; Gogotsi, Y.; Eklund, P.; et al. Transparent Conductive Two-Dimensional Titanium Carbide Epitaxial Thin Films. *Chem. Mater.* **2014**, *26* (7), 2374–2381.

(6) Barsoum, M. W. The MAX Phases : A New Class of Solids. *Progress in Solid State Chemistry*. 2000, pp 201–281.

(7) Wang, H.-W.; Naguib, M.; Page, K.; Wesolowski, D. J.; Gogotsi, Y. Resolving the Structure of $Ti_3C_2T_x$ MXenes through Multilevel Structural Modeling of the Atomic Pair Distribution Function. *Chem. Mater.* **2016**, *28* (1), 349–359.

(8) Er, D.; Li, J.; Naguib, M.; Gogotsi, Y.; Shenoy, V. B. Ti_3C_2 MXene as a High Capacity Electrode Material for Metal (Li, Na, K, Ca) Ion Batteries. *ACS Appl. Mater. Interfaces* **2014**, *6* (14), 11173–11179.

(9) Tang, Q.; Zhou, Z.; Shen, P. Are MXenes Promising Anode Materials for Li Ion Batteries? Computational Studies on Electronic Properties and Li Storage Capability of Ti_3C_2 and $Ti_3C_2T_x$ (X = F, OH) Monolayer. *J. Am. Chem. Soc.* **2012**, *134* (40), 16909–16916.

(10) Boota, M.; Anasori, B.; Voigt, C.; Zhao, M.-Q.; Barsoum, M. W.; Gogotsi, Y. Pseudocapacitive Electrodes Produced by Oxidant-Free Polymerization of Pyrrole between the Layers of 2D Titanium Carbide (MXene). *Adv. Mater.* **2016**, *28* (7).

(11) Lukatskaya, M. R.; Mashtalir, O.; Ren, C. E.; Dall'Agnese, Y.; Rozier, P.; Taberna, P. L.; Naguib, M.; Simon, P.; Barsoum, M. W.; Gogotsi, Y. Cation Intercalation and High Volumetric Capacitance of Two-Dimensional Titanium Carbide. *Science* **2013**, *341* (6153), 1502–1505.

(12) Wang, X.; Kajiyama, S.; Iinuma, H.; Hosono, E.; Oro, S.; Moriguchi, I.; Okubo, M.; Yamada, A. Pseudocapacitance of MXene Nanosheets for High-Power Sodium-Ion Hybrid Capacitors. *Nat. Commun.* **2015**, *6*, 1–6.

(13) Liang, X.; Garsuch, A.; Nazar, L. F. Sulfur Cathodes Based on Conductive MXene Nanosheets for High-Performance Lithium-Sulfur Batteries. *Angew. Chemie - Int. Ed.* **2015**, *54* (13), 3907–3911.

(14) Naguib, M.; Come, J.; Dyatkin, B.; Presser, V.; Taberna, P.-L.; Simon, P.; Barsoum, M. W.; Gogotsi, Y. MXene: A Promising Transition Metal Carbide Anode for Lithium-Ion Batteries. *Electrochem. commun.* **2012**, *16*, 61–64.

(15) Luo, J.; Zhang, W.; Yuan, H.; Jin, C.; Zhang, L.; Huang, H.; Liang, C.; Xia, Y.; Zhang, J.; Gan, Y.; et al. Pillared Structure Design of MXene with Ultralarge Interlayer Spacing for High-Performance Lithium-Ion Capacitors. *ACS Nano* **2017**, *11* (3), 2459–2469.

(16) Anasori, B.; Lukatskaya, M. R.; Gogotsi, Y. 2D Metal Carbides and Nitrides (MXenes) for Energy Storage. *Nat. Rev. Mater.* **2017**, *2* (2), 16098.

(17) Ren, C. E.; Hatzell, K. B.; Alhabeb, M.; Ling, Z.; Mahmoud, K. A.; Gogotsi, Y. Charge- and Size-Selective Ion Sieving Through $Ti_3C_2T_x$ MXene Membranes. *J. Phys. Chem. Lett.* **2015**, *6* (20), 4026–4031.

(18) Srimuk, P.; Halim, J.; Lee, J.; Tao, Q.; Rosen, J.; Presser, V. Two-Dimensional Molybdenum Carbide (MXene) with Divacancy Ordering for Brackish and Sea Water Desalination via Cation and Anion Intercalation. *ACS Sustain. Chem. Eng.* **2018**, acssuschemeng.7b04095.

(19) Peng, Q.; Guo, J.; Zhang, Q.; Xiang, J.; Liu, B.; Zhou, A.; Liu, R.; Tian, Y. Unique Lead Adsorption Behavior of Activated Hydroxyl Group in Two-Dimensional Titanium Carbide. *J. Am. Chem. Soc.* **2014**, *136* (11), 4113–4116.

(20) Yang, Y.; Umrao, S.; Lai, S.; Lee, S. Large-Area Highly Conductive Transparent Two-Dimensional Ti_2CT_x Film. *J. Phys. Chem. Lett.* **2017**, *8* (4), 859–865.

(21) Ying, G.; Dillon, A. D.; Fafarman, A. T.; Barsoum, M. W. Transparent, Conductive Solution Processed Spincast 2D Ti_2CT_x (MXene) Films. *Mater. Res. Lett.* **2017**, *5* (6), 391–398.

(22) Ali, A.; Belaidi, A.; Ali, S.; Helal, M. I.; Mahmoud, K. A. Transparent and Conductive $Ti_3C_2T_x$ (MXene) Thin Film Fabrication by Electrohydrodynamic Atomization Technique. *J. Mater. Sci. Mater. Electron.* **2016**, *27* (5), 5440–5445.

(23) Ying, G.; Kota, S.; Dillon, A. D.; Fafarman, A. T.; Barsoum, M. W. Conductive Transparent V_2CT_x (MXene) Films. *FlatChem* **2018**, *8*, 25–30.

(24) Ling, Z.; Ren, C. E.; Zhao, M.-Q.; Yang, J.; Giammarco, J. M.; Qiu, J.; Barsoum, M. W.; Gogotsi, Y. Flexible and Conductive MXene Films and Nanocomposites with High Capacitance. *Proc. Natl. Acad. Sci.* **2014**, *111* (47), 16676–16681.

(25) Han, M.; Yin, X.; Wu, H.; Hou, Z.; Song, C.; Li, X.; Zhang, L.; Cheng, L. Ti3C2MXenes with Modified Surface for High-Performance Electromagnetic Absorption and Shielding in the X-Band. *ACS Appl. Mater. Interfaces* **2016**, *8* (32), 21011–21019.

(26) Shahzad, F.; Alhabeb, M.; Hatter, C. B.; Anasori, B.; Man Hong, S.; Koo, C. M.; Gogotsi, Y. Electromagnetic Interference Shielding with 2D Transition Metal Carbides (MXenes). *Science* **2016**, *353* (6304), 1137–1140.

(27) Ma, Y.; Liu, N.; Li, L.; Hu, X.; Zou, Z.; Wang, J.; Luo, S.; Gao, Y. A Highly Flexible and Sensitive Piezoresistive Sensor Based on MXene with Greatly Changed Interlayer Distances. *Nat. Commun.* **2017**, *8* (1).

(28) Collini, P.; Kota, S.; Dillon, A. D.; Barsoum, M. W.; Fafarman, A. T. Electrophoretic Deposition of Two-Dimensional Titanium Carbide (MXene) Thick Films. *J. Electrochem. Soc.* **2017**, *164* (9), 573–580.

(29) Ghidiu, M.; Halim, J.; Kota, S.; Bish, D.; Gogotsi, Y.; Barsoum, M. W. Ion-Exchange and Cation Solvation Reactions in Ti_3C_2 MXene. *Chem. Mater.* **2016**, *28* (10), 3507–3514.

(30) Lerf, A.; Schoellhorn, R. Solvation Reactions of Layered Ternary Sulfides A_xTiS_2, A_xNbS_2, and A_xTaS_2. *Inorg. Chem.* **1977**, *16* (11), 2950–2956.

(31) Chipera, S. J.; Carey, J. W.; Bish, D. L. Controlled-Humidity XRD Analyses: Application to the Study of Smectite Expansion/Contraction. *Advances in X-ray Analysis*; Springer, **1998**; pp 713–722.

(32) Da Silva, G. J.; Fossum, J. O.; Dimasi, E.; Må, K. J.; Lutnaes, S. B. Synchrotron X-Ray Scattering Studies of Water Intercalation in a Layered Synthetic Silicate.

(33) Slade, P. G.; Quirk, J. P.; Norrish, K. Crystalline Swelling of Smectite Samples in Concentrated NaCI Solutions in Relation to Layer Charge. *Clays Clay Miner.* **1991**, *39* (3), 234–238.

(34) Come, J.; Black, J. M.; Lukatskaya, M. R.; Naguib, M.; Beidaghi, M.; Rondinone, A. J.; Kalinin, S. V.; Wesolowski, D. J.; Gogotsi, Y.; Balke, N. Controlling the Actuation Properties of MXene Paper Electrodes upon Cation Intercalation. *Nano Energy* **2015**, *17*, 27–35.

(35) Levi, M. D.; Lukatskaya, M. R.; Sigalov, S.; Beidaghi, M.; Shpigel, N.; Daikhin, L.; Aurbach, D.; Barsoum, M. W.; Gogotsi, Y. Solving the Capacitive Paradox of 2D MXene Using Electrochemical Quartz-Crystal Admittance and in Situ Electronic Conductance Measurements. *Adv. Energy Mater.* **2015**, *5* (1), 1–11.

(36) Kajiyama, S.; Szabova, L.; Iinuma, H.; Sugahara, A.; Gotoh, K.; Sodeyama, K.; Tateyama, Y.; Okubo, M.; Yamada, A. Enhanced Li-Ion Accessibility in MXene Titanium Carbide by Steric Chloride Termination. *Adv. Energy Mater.* **2017**, *7* (9), 1601873.

(37) Newbury, D. E. Mistakes Encountered during Automatic Peak Identification of Minor and Trace Constituents in Electron-Excited Energy Dispersive X-Ray Microanalysis. *Scanning* **2009**, *31* (3), 91–101.

(38) Hu, M.; Hu, T.; Li, Z.; Yang, Y.; Cheng, R.; Yang, J.; Cui, C.; Wang, X. Surface Functional Groups and Interlayer Water Determine the Electrochemical Capacitance of $Ti_3C_2T_x$ MXene. *ACS Nano* **2018**, acsnano.8b00676.

(39) Ying, Y.; Liu, Y.; Wang, X.; Mao, Y.; Cao, W.; Hu, P.; Peng, X. Two-Dimensional Titanium Carbide for Efficiently Reductive Removal of Highly Toxic Chromium(VI) from Water. *ACS Appl. Mater. Interfaces* **2015**, *7* (3), 1795–1803.

(40) Hope, M. A.; Forse, A. C.; Griffith, K. J.; Lukatskaya, M. R.; Ghidiu, M.; Gogotsi, Y.; Grey, C. P. NMR Reveals the Surface Functionalisation of Ti_3C_2 MXene. *Phys. Chem. Chem. Phys.* **2016**, *18* (7), 5099–5102.

(41) Ghidiu, M.; Kota, S.; Halim, J.; Sherwood, A. W.; Nedfors, N.; Rosen, J.; Mochalin, V. N.; Barsoum, M. W. Alkylammonium Cation Intercalation into Ti_3C_2 (MXene): Effects on Properties and Ion-Exchange Capacity Estimation. *Chem. Mater.* **2017**, *29* (3), 1099–1106.

(42) Swartzen-Allen, S. L.; Matijević, E. Surface and Colloid Chemistry of Clays. *Chem. Rev.* **1974**, *74* (3), 385–400.

Table of Contents Graphic